Journal of Machine Construction and Maintenance
QUARTERLY 1/2019(112)
ISSN 1232-9312
p. 31–38

Wojciech S. GUTOWSKI*, Phil S. CASEY, Sheng LI, Weidong YANG
CSIRO Manufacturing Flagship, Industrial Interfaces Group, Melbourne, Australia
* Corresponding author: Voytek.Gutowski@csiro.au

NANOSTRUCTURED FLEXIBLE FUNCTIONAL FILMS FOR ENERGY CONVERSION AND MANAGEMENT CSIRO MANUFACTURING FLAGSHIP

Key words: nanomaterials, energy conversion, vanadium dioxide, indium dioxide, phase transition materials, surface conductivity, photochromic windows, light-emitting devices.

Abstract: Understanding and controlling the capture and conversion of energy and the flow of electrical charges within the bulk and/or across surfaces of materials and interfaces is a focus of significant scientific and technological pursuit. Our paper focuses on nanomaterials and hybrid systems targeting the management of IR, UV, and RF radiation by absorption or reflection mechanisms. It is assisted by engineering the structure of certain nanomaterials and by charge transfer along functional interphases imparting surface conductivity to the originally non-conductive materials such as flexible polymeric films. The latter constitute principal scaffolds for a variety of advanced technology applications such as: energy harvesting, conversion and storage, e.g., solar cells, lithium ion batteries, supercapacitors, or hydrogen storage.

Nanostrukturalne elastyczne warstwy funkcjonalne do konwersji energii

Słowa kluczowe: nanomateriały, konwersja energii, dwutlenek wanadu, ditlenek indu, materiały przemiany fazowej, przewodnictwo powierzchniowe, okna fotochromowe, urządzenia emitujące światło.

Streszczenie: Zrozumienie i kontrolowanie wychwytywania i konwersji energii oraz przepływu ładunków elektrycznych w masie i/lub w poprzek powierzchni materiałów i międzyfazy jest przedmiotem znaczących osiągnięć naukowych i technologicznych. Nasz artykuł koncentruje się na nanomateriałach i systemach hybrydowych ukierunkowanych na wykorzystanie promieniowania IR, UV i RF za pomocą mechanizmów absorpcji lub odbicia. Pomaga mu w tym inżynieria struktury niektórych nanomateriałów i przenoszenie ładunku wzdłuż funkcjonalnych miedzyfaz, które nadają przewodność powierzchni pierwotnie nieprzewodzącym materiałom, takim jak elastyczne folie polimerowe. Te ostatnie stanowią główne rusztowania dla szeregu zaawansowanych zastosowań technologicznych takich, jak: zbieranie, przekształcanie i przechowywanie energii, np. ogniwa słoneczne, akumulatory litowo-jonowe, superkondensatory lub akumulatory wodoru.

Introduction

2-D and 3-D (2- / 3-dimensional) nanomaterials, in the form of nanoparticles, nanorods, nanowires, nanofibers, nanotubes, nano- or mesoporous frameworks play a critical role in the advancement of numerous advanced technologies. They differ from their micro-sized and bulk analogues, not only in the scale of dimensions, but also in the fact that they often exhibit new physical properties offering new technical applications [1].

With the size decrease, the percentage of atoms on the surface of a material drastically increases as does the surface-to-volume ratio. As highlighted by Chen et al, [2], whilst 100 nm particles have less than 0.2% of atoms located on their surface, for a 10 nm particle it is about 10%, whilst for a 2 nm particle, approximately 90% of the atoms that are surface-placed. The surface-exposed atoms are active and able to form bonds with adjacent molecules resulting in (i) an increased chemical activity, higher charge transport efficiency or the enhancement of other functional properties of a nanomaterial in comparison to its micro- and bulk equivalents, and (ii) interactions with adjacent particles to reduce the total energy of the system, and hence, stabilizing it.

Devices such as photovoltaic panels, display- or touch panels, solid-state lighting, and smart windows require the use of transparent materials which must be designed with in-built functionalities (as discussed below) and exhibit reliable performance. The latter is critically reliant on a tough (non-fragile) transparent nanoparticle-based coating permanently adhering to the surface of a flexible scaffold material, e.g., polymeric film, which may be subjected to severe bending and other hydro-thermo-mechanical stresses during the device service life. Hence, important applications discussed in this paper are 'flexible devices' made of thin, flexible, and transparent polymeric films for devices such as "roll-up" image displays, electroluminescent lighting panels replacing incandescent bulbs, smart windows, or printable sensors for tagging and tracking.

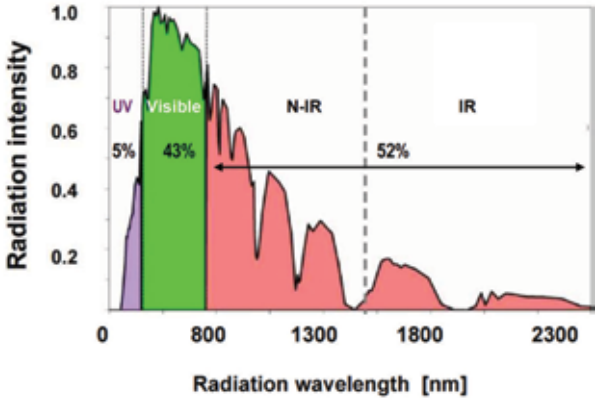

Fig. 1. Solar radiation energy distribution [%] and typical utilisation/conversion strategy: UV – absorption/ photovoltaic devices; Visible – energy switching (absorption and re-emission; IR – reflection or thermoelectric conversion

1. Infra-Red Fraction Of Solar Radiation: Incident Energy Management

The management and utilisation of solar radiation constitutes a significant target of scientific research. Spectral technologies have already demonstrated impressive outcomes utilised in flexible photovoltaic and electronics where light is converted to electrical energy [2]. By comparison, converting thermal energy embodied within the near infrared (NIR) and infra-red (IR) component (700–2500 nm) of solar radiation (see Figure 1) into other usable energy forms has received significantly less attention. Hence, the development of nanomaterials and coatings able to control the transmission and/or conversion of this energy by the use of specialty materials utilized in the form of thin functional film or additives is of significant practical interest.

Under the influence of electromagnetic radiation signals, e.g., IR, incident on, or propagating through a material, its constituents such as molecules or atoms oscillate and gain energy. Depending on the properties of a material, appropriate fractions of the flux of this radiation is reflected, transmitted, and/or alternatively attenuated by absorption or scattering. The fraction of energy absorbed or scattered internally is subsequently dissipated, as schematically illustrated in Figure 2: (i) within the material, manifesting itself as the absorbed thermal energy (A) heating the material, and (ii) emitted (E) from the glass panel.

1.1. Phase Transition Materials for management of IR radiation

One of particularly interesting approaches to the design of materials converting or mitigating transmission of energy embodied within the near infrared (N-IR) or IR band of solar radiation is through imparting a material's phase transition under the influence of an external stimulus such as temperature, which consequently triggers conversion of material's

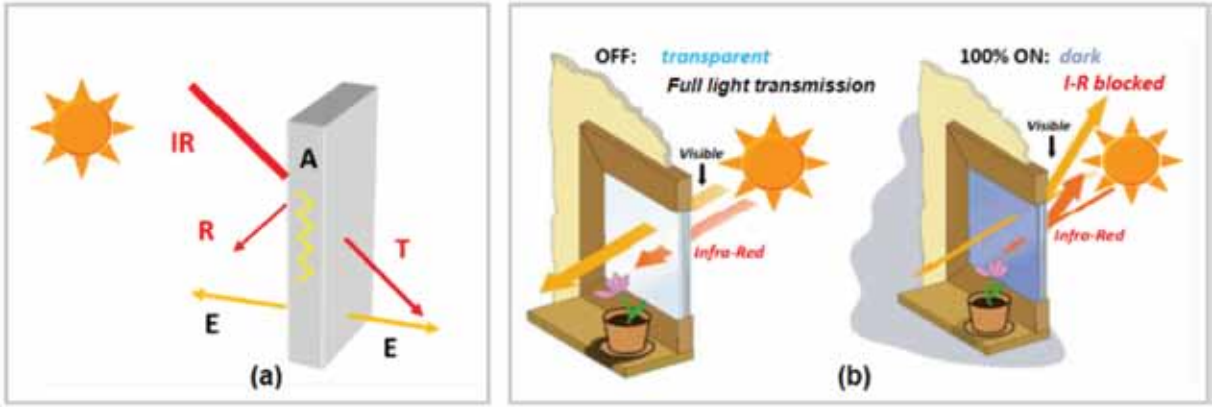

Fig. 2. (a) Performance factors of functional materials in thermo-chromic windows harnessing the IR fraction of solar radiation energy; R – reflectance; A – absorbance; T – transmittance; E – emissivity, (b) Thermo-chromic window modes of operation: *'off'* (full transparency) and *'on'* (I-R radiation blocking)

crystalline structure from semi-conductor to a metal. One of such materials, Vanadium (IV) oxide, VO_2, undergoes a temperature-controlled semiconductor-to-metal transition associated with a concomitant change in crystal symmetry. This phase transition, from semiconducting to metallic state, is associated with drastic increase in IR reflectivity, with no change observed regarding material transparency in the visible region of the spectrum. For pure, undoped VO_2, it occurs at phase transition temperature, T_C = 68°C, as shown in Figure 3 presenting the temperature dependence in electronic conductivity of pure VO_2, which can increase by up to 5 orders of magnitude [6] with simultaneous reduction in the transmission of IR. This has significant potential for applications such as thermochromic glazing [7], whose schematics are illustrated in Figure 2 above.

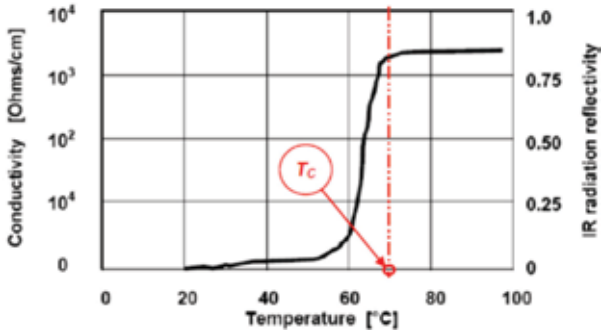

Fig. 3. Temperature dependence of conductivity and IR reflectivity of pure VO_2

2.2. The mechanism of phase transition in vanadium dioxide

Figure 4 illustrates the structure of VO_2. At low temperatures ($T < T_C$), the semiconducting VO_2 has a distorted rutile structure illustrated in Figure 4(b) with shorter distances between pairs of V atoms indicating metal-metal bonding. Above the phase transition temperature, T_C = 68°C, the structure changes (see Fig. 4c) to an undistorted tetragonal rutile structure with the metal-metal bonds broken causing a significant increase in electrical conductivity.

Structural transformation at T_C leading to changes in electrical and optical properties of VO_2 causes reconstruction of the material's electronic structure within picoseconds.

The mechanism of temperature-controlled phase transition from semiconductor-to-metal is not yet fully explained, but it is known to be associated with a concomitant change in crystal symmetry. Research carried out at Oak Ridge National Laboratory [4] demonstrated that it most likely might be caused by the formation of conductive nano-wires in VO_2, as illustrated in Figure 5 below.

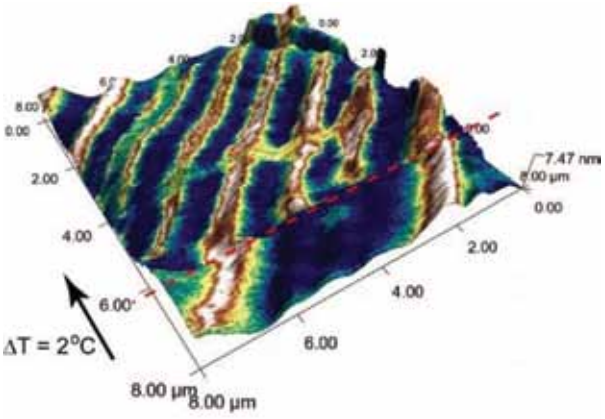

Fig. 5. Conductive nano-wires in VO_2 seen here as grey stripes [4]

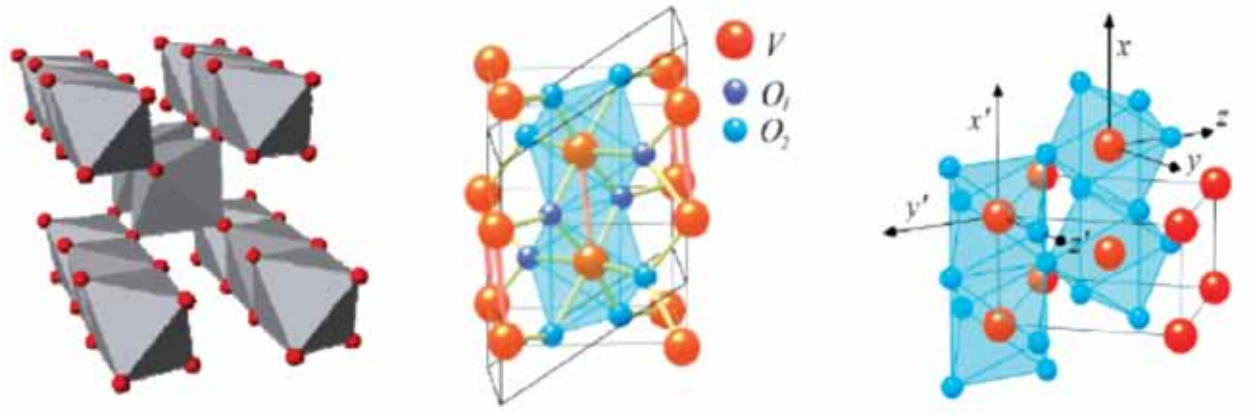

Fig. 4. (a) Schematic structure of pure VO_2; (b) Monoclonic (M_1) structure of VO_2 at $T < T_C$, vanadium atoms are depicted in red and oxygen atoms in a lighter colour; (c) The rutile structure of VO_2 at $T > T_C$ (adopted from [5])

2. Experimental: Materials, Analytical and Test Methods, Results

The key paths for synthesising vanadium dioxide are (i) chemical vapour deposition (CVD) to produce thin films [5, 10], (ii) sol-gel deposition via dip-coating, followed by calcination to also produce thin films [11, 12], or (iii) precipitation of an amorphous vanadium(IV) precursor (e.g., alkoxide) followed by calcination to produce small particles or nano-powders [13–15].

2.1. Preparation of Vanadium Dioxide

2.1.1. Synthesis of Pure Vanadium Dioxide, VO_2

Our method is based on a redox reaction utilising V_2O_5 and aspartic acid, both of which are readily available and relatively inexpensive. The process, see Figure 6(a) for its schematics, is carried out as follows [8]: A 2 h reflux of 0.9 or 1.0 g of vanadium pentoxide (Riedel de Haan) with 1.0 g of aspartic acid (Aldrich) in 50 mL of water purified with a Milli-Q filter was employed to reduce vanadium(V) oxide to a vanadium(IV) precursor. The resultant precipitate was filtered, washed with water, dried, and then calcined under argon in a tube furnace at 600 or 800°C for either 1 or 8 h. After calcining the gel-like intermediate, highly crystalline VO_2 nanoparticles were produced, as illustrated in Fig 6(b). The yields, calculated after calcination, were typically >80%.

Figure 7 below illustrates the N-IR reflectance of a thin composite film (VO_2 nanoparticles, as seen in Figure 6(b), in a matrix of a polyurethane coating) above and below the phase transition temperature. It can be seen from [5] that approximately 80% of IR radiation in the waveband above 1200 nm is reflected by VO_2 above the phase transition temperature T_C = 68°C.

2.1.2. Synthesis of tungsten-doped VO_2

For practical applications, the temperature at which transition occurs needs to be lowered to more useful ranges (25–30°C), which is accomplished by doping the VO_2 with a secondary cation such as W, Mo or Cr, as illustrated in Figure 8.

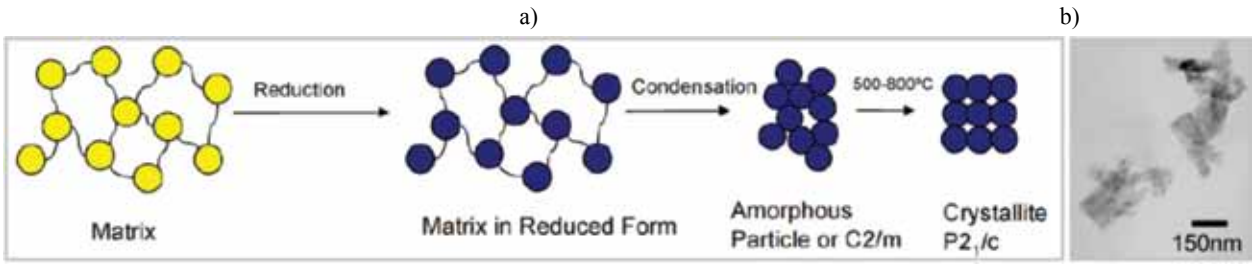

Fig. 6. Schematics of synthetic route based on a redox reaction mechanism using V_2O_5 and aspartic acid [8]

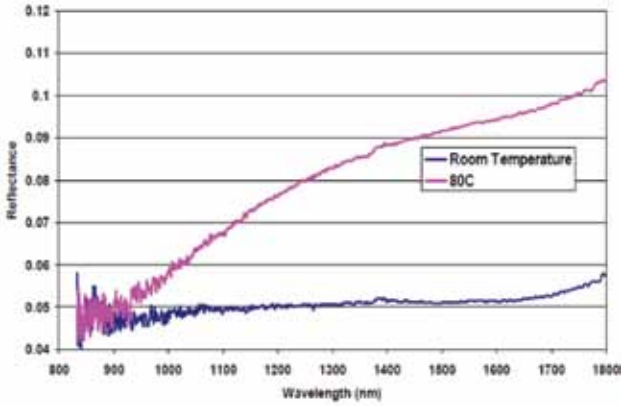

Fig. 7. IR diffuse reflectance spectra of VO_2 above and below transition temperature [9]

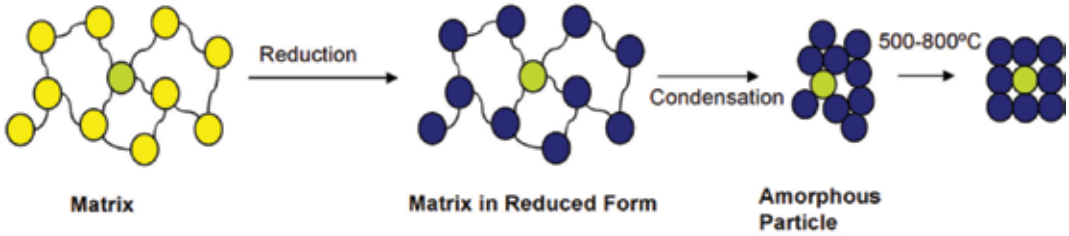

Fig. 8. Schematics of synthetic route utilising V_2O_5 for sol-gel preparation of tungsten-doped VO_2

As presented in Figure 9, the increase of concentration of the dopant (tungsten) reduces the transition temperature (T_C) from 68°C for undoped VO_2 to as low as 22°C at 2% W.

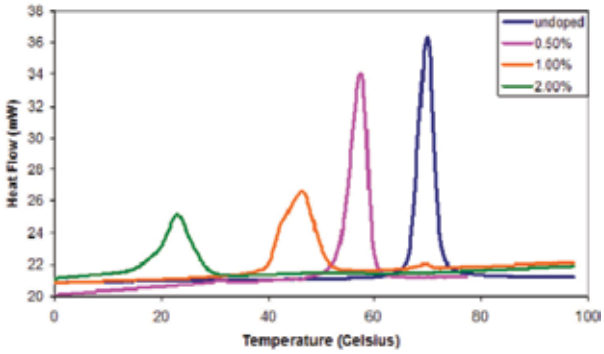

Fig. 9. Enthalpy of insulator-to-metal transition for a series of VO_2 nanoparticles doped with increasing amounts of W (0.0, 0.5, 1.0, 2.0 wt%) [9]

2.2. Analytical methods and equipment

2.2.1. Scanning Electron Microscopy (SEM)

A Philips XL30 FEG SEM was used for acquiring SEM images. Samples were mounted on-edge. Imaging of the coating structure was performed on uncoated samples, whilst a carbon coating was applied to the samples to the required performing thickness measurements.

2.2.2. Transmission Electron Microscopy (TEM)

The samples were deposited on 200 mesh carbon-coated copper grids, and microscopy was performed on a Philips CM30 transmission electron microscope operating at an accelerating voltage of 200 kV.

3.2.3 Differential Scanning Calorimetry (DSC)

Calorimetry experiments were performed on a Perkin-Elmer Pyris 1 calorimeter using hermetically sealed aluminum pans, between 20 and 100°C at a scan rate of 5°C/min under nitrogen.

3.2.4. Surface resistivity determination

The sheet resistivity (R_s), the sheet charge carrier density (n_s), and the charge carrier mobility (μ_H) were determined using a HEM 2000 Hall Effect Measurement system. This measurement system utilises a 4-point configuration, thus providing redundancy and the appropriate geometric pattern to reduce errors and eliminate contact resistance between the probes and sample. Silver loaded epoxy was used to make ohmic contacts to the corners of the films. During each set of measurements, a commercially available ITO coated glass sample (Presizion Glass Optik (PGO)) was measured as a reference.

2.2.5. UV-visible spectra

These were acquired on a Varian CARY 3 spectrophotometer. All spectra were collected over the range of 200–800 nm with ~1nm resolution.

2.2.6. Transmittance of ITO film.

The transparency of the ITO film was measured by UV-visible spectrometer. In this analysis, the dispersion was spin-coated onto cleaned quartz (3-layered coating at 1000RPM, and 4 layered coatings at 2000RPM).

3. Electro-conductive ito-based coatings for optoelectronic devices

3.1. Properties of indium tin oxide (ITO)

Indium tin oxide (ITO) is one of most important materials for multi-functional devices utilising opto-electronic properties of this material. In the form of thin continuous films, it exhibits optical transparency at the level of 80 to 95%, high electronic conductivity, and the ability to reflect infrared radiation. Due to the above properties, thin ITO films are particularly suitable for fabrication of the following: (i) transparent electrodes for thin-film electro-luminescent displays and electro-chromic devices; (ii) transparent conductive coatings for radiation detectors; (iii) solar cells and energy storage devices; and, (iv) opto-electro-chromic coatings for effective shielding solar radiation through targeting UV absorption and reflection of I-R radiation.

Pure indium oxide (In_2O_3) is a wide-gap n-semiconductor whose relatively high conductivity is attributed to the presence of doubly charged oxygen vacancies (V_o^{**}), see Figure 10, which provide a conduit for the charge transfer. Doping indium oxide, e.g., by Sb, Sn of F significantly increases its conductivity. During incorporation of the dopant, e.g., tin, the atoms

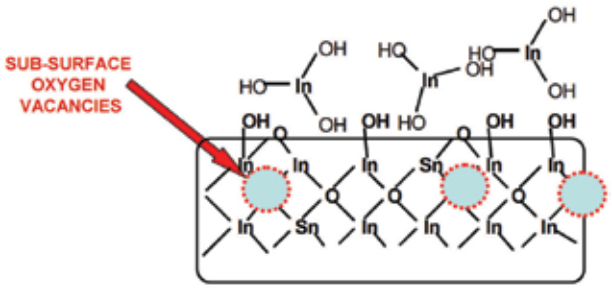

Fig. 10. Schematics of the ITO surface and sub-surface structure illustrating the termination of the bixebyte lattice with both, bridging and non-bridging oxygen atoms (oxygen vacancies), and hydroxylated indium, in $(OH)_3$, providing suitable sites for the attachment of organic molecules such as dispersants and organic dopants

enter ITO lattice (e.g., as Sn^{4+} ions) substituting In^{3+} ions in the cation sites, and act as *n*-type donors. As the Sn contents increases, the unit cell is enlarged and the host lattice becomes disturbed. The addition of tin atoms increases carrier concentration, and hence conductivity, but reduces charge mobility due to the lattice distortion.

The following challenges need to be overcome in the fabrication of effective transparent electro-conductive ITO coatings for optoelectronic applications:

- The minimisation of the size of dispersant molecules to reduce percolation threshold arising from the separation of individual ITO nano-particles,
- The substitution of non-conductive dispersant molecules by those containing charge-conducting moieties, and
- Grafting electro-conductive molecules onto non-bridging oxygen atoms within oxygen vacancies to prevent gradual deactivation of the conductive lattice (Figure 10 and Figure 12).

3.2. Transparency of ITO film

The transparency of the ITO films spin-coated onto cleaned quartz (1 to 4 layers) was measured by UV-visible spectrometer. The data illustrated in Figure 11 demonstrate that our ITO films (applied from dispersion) show very high transparency. The transmittance is approximately 90% for 3 or 4 layers. Table 3 lists the transmittance of ITO films at 550 nm.

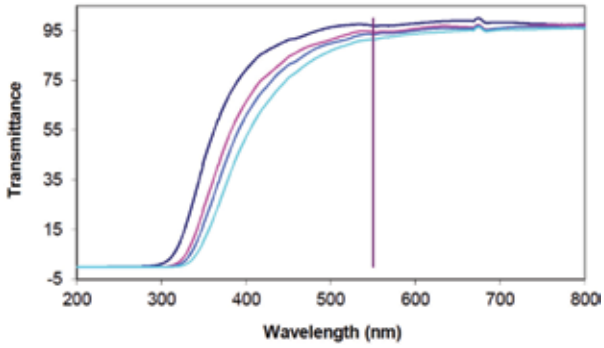

Fig. 11. Transmittance spectra of ITO films coated at 2000 RPM as 1 to 4 layer structures

3.3. Conductivity of ITO films

Experimental data presented in Figure 12 demonstrate the levels of the conductivity of printable nano-oxide films as follows: commercially available ITO coatings, commercial ATO coating, and 2 new-generation CSIRO coatings with ITO nano-particles doped by self-assembled electro-conductive organic molecules.

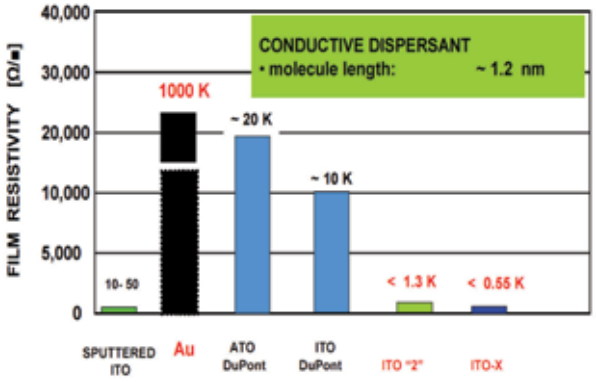

Fig. 12. Comparative data on conductivity of printable nano-oxide films on a flexible transparent PET substrate (30 µm): commercially available ITO coatings, ATO coating and a new generation CSIRO coating with ITO nano-particles doped by self-assembled electro-conductive organic molecules

The graph in Figure 13 also demonstrates that the functionalization of ITO surface with self-assembled molecules equipped with charge-conducting moieties leads to a significant improvement in the stability of ITO films. This feature is demonstrated through a noticeable reduction of the rate of the conductivity deterioration of our surface-modified ITO films exposed to ambient air. Whilst our ITO film retains conductivity at the level of 1650 Ohms/square after a 50-day work period in ambient air environment, the commercial ITO films illustrated in Figure 12 suffer a serious increase of their resistivity from the initial 10 kΩ/square to approx. 40––45 kΩ/square after just 30 days of work in ambient air.

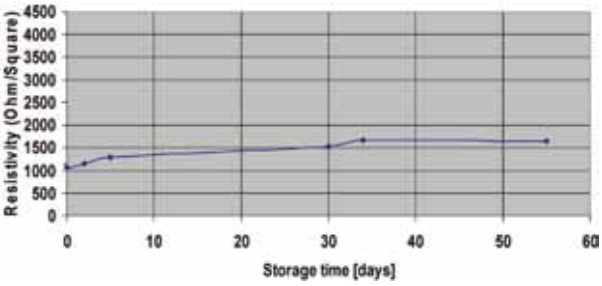

Fig. 13. Stabilisation of long-term conductivity of thin ITO film doped by self-assembled organic electro-conductive molecules

3.4. Practical utilisation of flexible ITO film in light-emitting panels

Figure 14 below presents the schematic structure [see panel (a)] and a photo of flexible light emitting panel fabricated with the use of thin PET film (40 µm) utilising ITO denoted *'ITO-2'* in Figure 12 and 13 (Note: surface resistivity = inverse of surface conductivity).

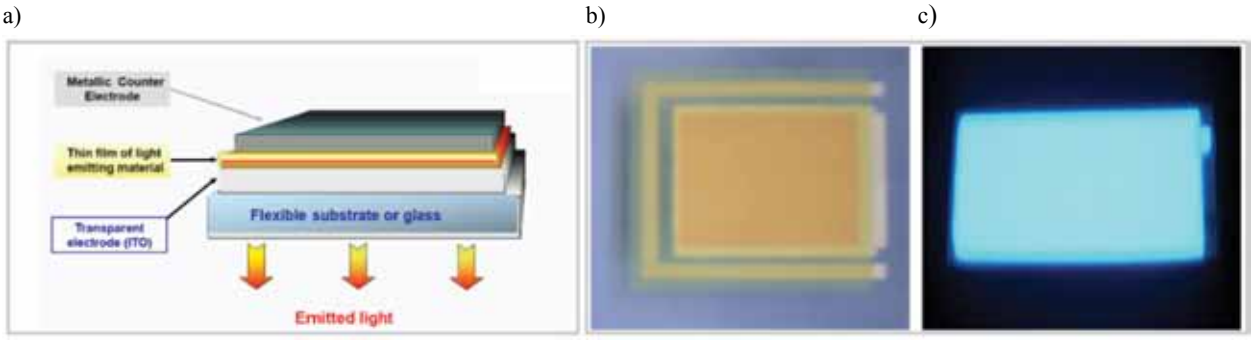

Fig. 14. (a) Schematic structure and photos of flexible light emitting panel fabricated with the use of thin PET film (40 µm) utilising ITO denoted *'ITO-2'*, as per surface resistivity (inverse conductivity) illustrated in Figures 11 and 12: (b) an unrolled device, and (c) a switched-on light-emitting panel

Conclusions

1. Flexible functional devices comprising transparent nanoparticles synthesised in this work and subsequently applied as flexible coatings covalently integrated with the transparent polymeric scaffold (PET film, 40 µm) were successfully fabricated for the following energy conversion applications: (i) thermochromic films based on VO_2, (ii) transparent ITO films, and (iii) light-emitting devices.
2. A facile process developed in this work facilitated the synthesis of transparent and flexible VO_2 films exhibiting controllable phase transition temperature in the range of 17 to 68°C.
3. A novel process developed in this work for high-conductivity transparent ITO-based films is demonstrated to achieve the following: (i) surface conductivity about 10-fold higher than commodity ITO-based printing films; (ii) long-term retention of ITO surface conductivity, which is known to rapidly deteriorate in commercially available ITO coatings and inks; and, (iii) excellent covalent integration and flexibility of the printed ITO ink, which can be bent multiple times without film fracture or separation form the flexible substrate surface.

References

1. Zhang Q., Uchaker E., Candelaria S.L., Cao G.: Nanomaterials for energy conversion and storage. *Chemical Society Reviews*, 2013, 42, pp. 3127–3171.
2. Chen X., Grätzel C.Li.M., Kostecki R., Mao S.S.: Nanomaterials for renewable energy production and storage. *Chemical Society Reviews,* 2012, 41, pp. 7909–7937.
3. Tselev A., Luk'yanchuk I.A., Ivanov I.N., Budai J.D., Tischler J.Z., Strelcov E., Kolmakov A., Kalinin S.V.: Symmetry Relationship and Strain-Induced Transitions between Insulating M1 and M2 and Metallic R phases of Vanadium Dioxide. *Nano Letters*, 2010, 10 (11), pp. 4409–4416.
4. Oak Ridge National Laboratory: *Scientists crack materials mystery in vanadium dioxide*. [Online]. 2010. [Accessed 26 November 2018]. Available from: https://www.ornl.gov/news/ornl-scientists-crack-materials-mystery-vanadium-dioxide
5. Warwick M.E.A., Binions R.: Advances in thermochromic vanadium dioxide films. *Journal of Materials Chemistry A*, 2014, 2, pp. 3275–3292.
6. Berglund C.N., Guggenheim, H.J.: Electronic Properties of VO_2 near Semiconductor-Metal Transition. *Physical Review,* 1969, 185(3), pp. 1022–1033.
7. Manning T.D., Parkin I.P., Pemble M.E., Sheel D., Vernadou D.: Intelligent window coatings: Atmospheric pressure chemical vapor deposition of tungsten-doped vanadium dioxide. *Chemistry of Materials,* 2004, 16, pp. 744–749.
8. Booth J., Casey P.S.: Production of VO_2 M1 and M2 Nanoparticles and Composites and the Influence of the Substrate on the Structural Phase Transition. *ACS Applied Materials & Interfaces*, 2009, 1(9), pp. 1899–1905.
9. Casey P.S.: Towards The Development of Advanced Thermally Responsive Coatings: From IR Control (Passive and Active) To Thermoelectric. In: *European Coatings Conference "Sustainable Coatings", 18–19th June 2013, Düsseldorf.*
10. Manning T.D., Parkin I.P., Clark R.J.H., Sheel D., Pemble M.E., Vernadou D.: Intelligent Window Coatings: Atmospheric Pressure Chemical Vapour Deposition of Vanadium Oxides. *Journal of Materials Chemistry*, 2002, 12(10), pp. 2936–2939.
11. Lu S., Hou L., Gan F.: Surface analysis and phase transition of gel-derived VO2 thin films. *Thin Solid Films,* 1999, 353(1–2), pp. 40–44.
12. Hanlon T.J., Coath J.A., Richardson M.A.: Molybdenum-doped vanadium dioxide coatings on glass produced by the aqueous sol–gel method. *Thin Solid Films,* 2003, 436(2), pp. 269–272.

13. Xu C., Ma L., Liu X., Qiu W., Su Z.: A novel reduction–hydrolysis method of preparing VO_2 nanopowders. *Materials Research Bulletin*, 2004, 39(7–8), pp. 881–886.
14. Shi J., Zhou S., You B., Wu L.: Preparation and thermochromic property of tungsten-doped vanadium dioxide particles. *Solar Energy Materials and Solar Cells,* 2007, 91(19), pp. 1856–1862.
15. Peng Z., Jiang W., Liu H.: Synthesis and Electrical Properties of Tungsten-Doped Vanadium Dioxide Nanopowders by Thermolysis. *Journal of Physical Chemistry C,* 2007, 111(3), pp. 1119–1122.